2024 IEEE/ASME International Conference on Advanced Intelligent Mechatronics (AIM)
July 15-19, 2024. Boston, MA, USA

Gravity Compensation Mechanism Inspired by Sauropods' Skeleton

Ryotaro Kayawake, Kazuki Abe, Masahiro Watanabe, Kenjiro Tadakuma, and Satoshi Tadokoro

***Abstract*— We propose a gravity compensation mechanism that combines practical compensation performance and a simple structure inspired by the skeleton of sauropods. Conventional gravity compensation mechanisms typically involve complex structures and design theories to be unaffected by variations in posture and fluctuations in self-weight induced by external loads. In considering a simpler structure, we focused on the simple gravity compensation functionality observed in sauropods, a particularly gigantic group of dinosaurs characterized by their long necks and tails, making them the largest terrestrial animals in history, and referred to their skeleton. Our proposed method emphasizes simplicity over strict compensation mechanisms, employing a straightforward structure of wires aligned with the articulated links. In this paper, we demonstrate the mechanism's compensation performance, showing how the gravity compensation ratio varies with different postures through simulation. Additionally, we fabricated a prototype to test the compensation effect, further verifying the effectiveness of our proposed mechanism.**

I. Introduction

Multi-joint robot arms operating against gravity require a compensatory torque to counteract their own weight during operation. Utilizing the actuator output for both the intended movement and compensatory torque raises concerns regarding the increase in energy consumption. Additionally, unforeseen circumstances such as power failure pose a risk of limpness, making the arm unsafe to use as a collaborative tool.

A variety of mechanisms have been proposed to compensate for the influence of self-weight on a robot arm without an external energy supply. The primary gravity compensation mechanisms include counterweight, spring, and buoyancy methods. The counterweight method, which involves compensating for the gravitational potential of the self-weight with a counterweight, has a simple principle and the ability to cancel moments around a support point [1][2]. However, this approach increases mass and moment of inertia, making the robot arm less responsive. The spring method, in contrast, utilizes the elastic potential of the springs to offset compensates the gravitational potential without reducing the responsiveness [3][4]. Nevertheless, a conversion mechanism is required because of the linear nature of the gravitational potential with respect to the displacement and the nonlinear nature of the elastic potential. The buoyancy method compensates for the gravitational potential by using the buoyancy potential of the gas filled in the robot. Although this method allows the development of a simple and lightweight robot arm, the arm is limited to exploratory applications [5].

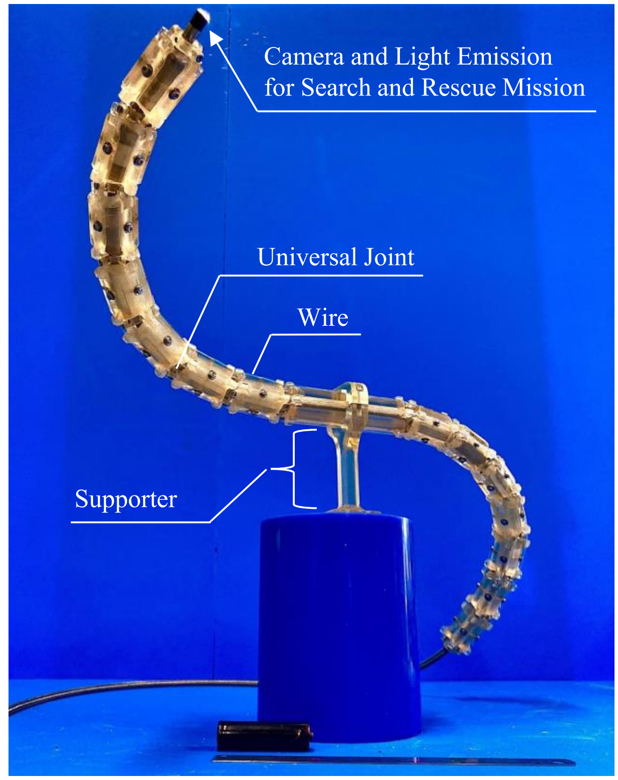

Figure 1. Prototype of the proposed mechanism

An optimal gravity compensation mechanism must be unaffected by variations in posture and fluctuations in self-weight induced by external loads. Several parallel links, noncircular pulleys, and cams with gravity compensation mechanisms have been proposed to counteract posture changes [2][6][7][8]. Another reported mechanism employs embedded springs to counteract the changes in self-weight [9]. If the acceptance of human assistance is acknowledged, structures that facilitate the replacement of components according to circumstances also tolerate changes in self-weight and posture [10]. However, strict adherence to these requirements typically imposes numerous design constraints. Conventional mechanisms that satisfy these criteria typically involve complex structures and design theories. To the best of our knowledge, examples of sufficiently simple structures have not been developed.

Structures akin to gravity compensation mechanisms are not exclusive to artificial constructs; they also manifest themselves in the natural world. A prime example is the

Ryotaro Kayawake and Satoshi Tadokoro are with the Graduate School of Information Sciences, Tohoku University, Japan.
Kazuki Abe, Masahiro Watanabe and Kenjiro Tadakuma,are with the Graduate school of Engineering Science, Osaka University.
(Corresponding author: Kenjiro Tadakuma, email: tadakuma@rm.is.tohoku.ac.jp).

sauropod [11][12]—a particularly gigantic group of dinosaurs characterized by a long neck and tail, making them the largest terrestrial animals in history. Sustaining the elongated necks and tails of sauropods required immense biological energy [13]. Consequently, it has been hypothesized that sauropods possessed gravity compensation functionality and maintained their posture through tension in the ligaments [12][14]. Simple gravity compensation mechanisms can be found in living organisms.

In this study, a gravity compensation mechanism that combines practical compensation functionality and a simple structure inspired by the skeleton of a sauropod is proposed (Fig. 1). The proposed mechanism adopts a counterweight-style design featuring straightforward construction achieved by connecting identically shaped links through wires. Simplicity is emphasized rather than strict compensation functionality; therefore, simulations were conducted to assess its practical compensatory capabilities.

II. Basic Principle

A. Construction of proposed mechanism

The proposed mechanism was constructed by connecting multiple links, each with the same shape, resembling a sauropod neck and tail (see Fig. 2). Universal joints are utilized between the links. When counting the joints starting from the central link as zero, the links with the same number were connected by wires. Each wire has a constant length when the proposed mechanism is not bent. For example, the red wire (heavy line) connects the joints labeled 3. Four wires are arranged for each link pair, allowing the transmission of rotations in the yaw and pitch directions. Viewed from the central link, one set of links is referred to as the active link, and the other set is referred to as the passive link. When the joint angle of the active links changes, the tension in the wires causes corresponding changes in the joint angles of the passive links. As the joint of the active link rotates in the direction of increasing potential, the corresponding joint of the passive link rotates to decrease the potential. Therefore, the proposed mechanism achieves gravity compensation as the entire system. Additionally, placing the actuator on the 0th link and actuating the wires allows active bending without increasing the moment of inertia [15].

B. Forward kinematics of individual joint

The derivation process of forward kinematics for an individual joint is presented. We consider the stationary orthonormal bases $\boldsymbol{i}$, $\boldsymbol{j}$, and $\boldsymbol{k}$ and denote the wire attachment positions of the active joint as $\boldsymbol{r}_1$, $\boldsymbol{r}_2$, $\boldsymbol{r}_3$, and $\boldsymbol{r}_4$ (see Fig. 3). When an active joint is rotated in the pitch direction by θ and in the yaw direction by φ, the position vectors $\boldsymbol{r}_2$ and $\boldsymbol{r}_4$, as observed from the stationary coordinate system, shift to $\boldsymbol{r}_2^{\prime}$ and $\boldsymbol{r}_4^{\prime}$, respectively, as expressed by the following equations:

$$\boldsymbol{r}_2^{\prime} = Rot[\boldsymbol{k}, \varphi] Rot[\boldsymbol{i}, \theta] \boldsymbol{r}_2 \tag{1}$$

$$\boldsymbol{r}_4^{\prime} = Rot[\boldsymbol{k}, \varphi] Rot[\boldsymbol{i}, \theta] \boldsymbol{r}_4 \tag{2}$$

where $Rot[\widehat{\boldsymbol{\omega}}, \vartheta]$ represents the rotation matrix for an angle ϑ around the axis $\widehat{\boldsymbol{\omega}}$. This completes the derivation of forward kinematics for an individual joint. The lengths of the wires placed between the active joints l_{12} and l_{34} can be expressed as follows:

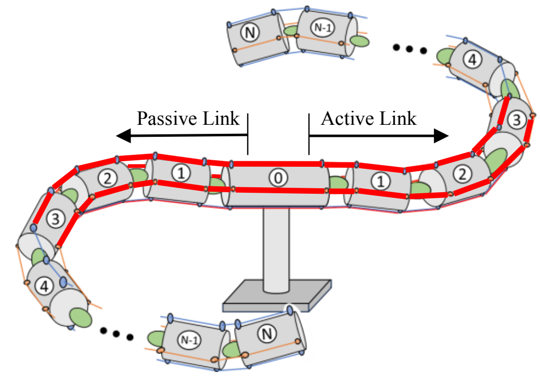

Figure 2. Construction of the proposed mechanism and link numbering

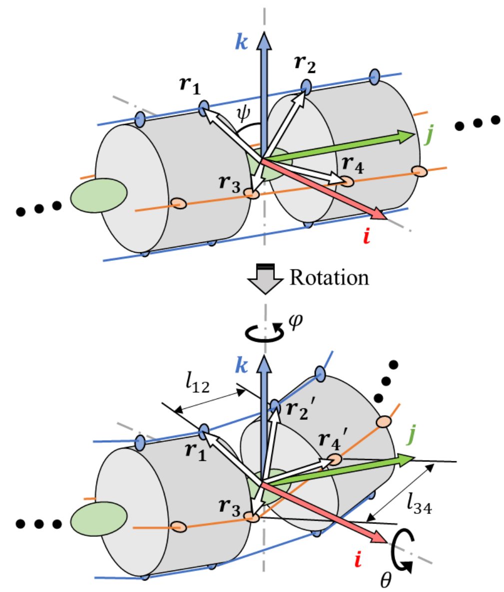

Figure 3. Definitions of the joint parameters and how they change

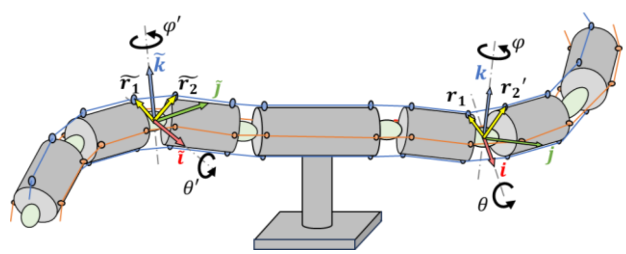

Figure 4. Correspondence between active and passive joints numbering

Figure 1

$$l_{12} = \|\boldsymbol{r}_2^{\prime} - \boldsymbol{r}_1\| \tag{3}$$

$$l_{34} = \|\boldsymbol{r}_4^{\prime} - \boldsymbol{r}_3\|, \tag{4}$$

where $\widetilde{r}_1$, $\widetilde{r}_2$, $\widetilde{r}_3$, and $\widetilde{r}_4$ denote the wire attachment positions of the passive joint. Additionally, $-\widetilde{\theta}$ and $-\widetilde{\varphi}$ represent the rotational angles for the pitch and yaw, respectively, of the passive joint caused by the rotation of the active joint (see Fig. 4). The position vectors $\widetilde{r}_2$ and $\widetilde{r}_4$ are then shifted to $\widetilde{r_2}'$ and $\widetilde{r_4}'$, as follows:

$$\widetilde{\boldsymbol{r}_2}' = Rot[\boldsymbol{k}, -\tilde{\varphi}]Rot[\boldsymbol{i}, -\tilde{\theta}]\tilde{\boldsymbol{r}}_2 \tag{5}$$

$$\boldsymbol{r}_4' = Rot[\boldsymbol{k}, -\varphi]Rot[\boldsymbol{i}, -\theta]\boldsymbol{r}_4. \tag{6}$$

In this case, the lengths of the wires placed between the passive joints, which are denoted as $\widetilde{l_{12}}$ and $\widetilde{l_{34}}$, can be expressed as follows:

$$\widetilde{l_{12}} = \|\widetilde{\boldsymbol{r}_2}' - \widetilde{\boldsymbol{r}_1}\| \tag{7}$$

$$\widetilde{l_{34}} = \|\widetilde{\boldsymbol{r}_4}' - \widetilde{\boldsymbol{r}_3}\|. \tag{8}$$

Because the lengths of the wires are constant before and after the joint rotations, the following relationship can be used:

$$l_{12} + l_{34} = 4r\sin\psi \tag{9}$$

$$\widetilde{l_{12}} + \widetilde{l_{34}} = 4r\sin\psi \tag{10}$$

$$\|\boldsymbol{r}_i\| = \|\tilde{\boldsymbol{r}}_i\| = r \ (i = 1 \cdots 4) \tag{11}$$

$$r\cos\psi = \boldsymbol{r}_i \cdot \boldsymbol{k} = \tilde{\boldsymbol{r}}_i \cdot \boldsymbol{k} \ (i = 1 \cdots 4). \tag{12}$$

By eliminating the rotation angles θ and φ from equations (9) and (10), the rotation angles $\tilde{\theta}$ and $\tilde{\varphi}$ for the passive joint are computed. However, as the above equations cannot be solved analytically, numerical methods such as Newton's method are required. The joint angles θ, φ, $\tilde{\theta}$, and $\tilde{\varphi}$ must satisfy the following equations for constructing an ideal gravity compensation mechanism.

$$\theta = \tilde{\theta} \tag{13}$$

$$\varphi = \tilde{\varphi}. \tag{14}$$

The only solution that satisfies equations (13) and (14) is $\theta = \varphi = 0$. This indicates that the proposed mechanism does not theoretically possess exact gravity compensation functionality when its posture changes from the initial state. The differences in angles between the active and passive joints, which are denoted as $\Delta\theta$ and $\Delta\varphi$, are defined as

$$\Delta\theta = |\theta' - \theta| \tag{15}$$

$$\Delta\varphi = |\varphi' - \varphi|. \tag{16}$$

C. Forward kinematics and gravitational potential of proposed mechanism

A derivation of the overall forward kinematics of the proposed mechanism is presented. The unit vectors $\boldsymbol{i}_n$, $\boldsymbol{j}_n$, and $\boldsymbol{k}_n$ denote the stationary orthonormal base for the n^{th} joint, and the homogeneous transformation matrix is defined as

$$T[\widehat{\boldsymbol{\omega}}, \vartheta, \boldsymbol{p}] = \begin{bmatrix} Rot[\widehat{\boldsymbol{\omega}}, \vartheta] & \boldsymbol{p} \\ \boldsymbol{0}^T & 1 \end{bmatrix}. \tag{17}$$

The relationship between the vectors ${}^{n}\boldsymbol{r}$ and ${}^{n+1}\boldsymbol{r}$ is computed as

$${}^{n}\boldsymbol{r} = T[\boldsymbol{k}_n, \varphi_n, \boldsymbol{0}]T[\boldsymbol{i}_n, \theta_n, \boldsymbol{0}]T[\boldsymbol{j}_n, 0, l\boldsymbol{j}_{n+1}]\,{}^{n+1}\boldsymbol{r}, \tag{18}$$

where ${}^{n}\boldsymbol{r}$ is a given vector $\boldsymbol{r}$ observed from the nth joint, ${}^{n+1}\boldsymbol{r}$ is observed from the $(n+1)$th joint, and l represents the length of the joint. Equation (18) expresses the overall forward kinematics of the proposed mechanism. The position of the center of mass of the n^{th} joint, i.e., $\boldsymbol{r}_{Gn}$, is obtained as follows:

$$\boldsymbol{r}_{Gn} = T_1 T_2 \cdots T_n \begin{bmatrix} -\frac{l}{2}\boldsymbol{j}_n \\ 1 \end{bmatrix} = \left[\prod_{i=1}^{k} T_i\right] \begin{bmatrix} \frac{l}{2}\boldsymbol{j}_n \\ 1 \end{bmatrix} \tag{19}$$

$$T_n[\widehat{\boldsymbol{\omega}}, \vartheta, \boldsymbol{p}] = T[\boldsymbol{k}_n, \varphi_n, \boldsymbol{0}]\, T[\boldsymbol{i}_n, \theta_n, \boldsymbol{0}]T[\boldsymbol{j}_n, 0, l\boldsymbol{j}_{n+1}]. \tag{20}$$

Therefore, the total gravitational energy U that the active joint receives is computed as

$$U = mg[\boldsymbol{k}_1{}^T \quad 1] \sum_{k=1}^{N} \left[\prod_{i=1}^{k} T_i\right] \begin{bmatrix} \frac{l}{2}\boldsymbol{j}_n \\ 1 \end{bmatrix}. \tag{21}$$

where m represents the mass of each joint, and g represents the gravitational acceleration.

D. Gravity compensation ratio of proposed mechanism and its calculation

The gravity compensation ratio ε for the proposed mechanism is defined as

$$\varepsilon = \left(1 - \frac{\Delta U}{U}\right), \tag{22}$$

where ΔU represents the energy received by the proposed mechanism from gravity when gravity compensation is performed, and U represents the energy received from gravity without compensation. ΔU is computed using the error propagation law.

$$\Delta U = \sqrt{\sum_{k=1}^{N} \left\{ \left(\frac{\partial U}{\partial \theta_k}\right)^2 \Delta\theta_k{}^2 + \left(\frac{\partial U}{\partial \varphi_k}\right)^2 \Delta\varphi_k{}^2 \right\}}. \tag{23}$$

Here, $\Delta\theta_k$ and $\Delta\varphi_k$ represent the angular differences between the kth active joint and the corresponding passive joint. However, there is no need to calculate the partial derivatives directly in equation (23); they are obtained as follows:

$$\frac{\partial U}{\partial \theta_n} = mg[\boldsymbol{k}_1 \quad 1] \sum_{k=n}^{N} \left[\prod_{i=1}^{k} \left\{\delta(i-n)\left(\frac{\partial T_n}{\partial \theta_n} - T_n\right) + T_i\right\}\right] \begin{bmatrix} \frac{l}{2}\boldsymbol{j}_n \\ 1 \end{bmatrix} \tag{24}$$

$$\frac{\partial U}{\partial \varphi_n} = mg[\boldsymbol{k}_1 \quad 1] \sum_{k=n}^{N} \left[\prod_{i=1}^{k} \left\{\delta(i-n)\left(\frac{\partial T_n}{\partial \varphi_n} - T_n\right) + T_i\right\}\right] \begin{bmatrix} \frac{l}{2}\boldsymbol{j}_n \\ 1 \end{bmatrix} \tag{25}$$

$$\frac{\partial T_n}{\partial \theta_n} = \begin{bmatrix} \frac{\partial}{\partial \theta_n} Rot[\widehat{\boldsymbol{\omega}'}, \vartheta'] & \boldsymbol{p}' \\ \boldsymbol{0}^T & 1 \end{bmatrix} \tag{26}$$

$$\frac{\partial T_n}{\partial \varphi_n} = \begin{bmatrix} \frac{\partial}{\partial \varphi_n} Rot[\widehat{\boldsymbol{\omega}'}, \vartheta'] & \boldsymbol{p}' \\ \boldsymbol{0}^T & 1 \end{bmatrix}, \tag{27}$$

where δ is the Kronecker delta, which is defined as

$$\delta(x) = \begin{cases} 1 \ (x = 0) \\ 0 \ (x \neq 0) \end{cases}. \tag{28}$$

III. Simulations

A. Relationship between position of bending joint and gravity compensation ratio

Simulations were conducted to investigate the effects of the errors on gravity compensation ratio expressed by equations (15) and (16). Initially, the relationship between the positions of the rotating joint and the gravity compensation ratio was examined (see Fig. 5). Consider the case where only the nth joint is rotated by the angle θ_n (in degrees) calculated using equation (29) in the vertical direction.

$$\theta_n = \delta(n - k) \cdot 18. \tag{29}$$

In the simulations, the values of the link length l and number of joints N were consistent with those used in the actual prototype (refer to Chapter 4). The simulation results with k varying from 1 to 7 indicate that for motion in the vertical plane, bending the tipper joint leads to a higher gravity compensation ratio ε (see Fig. 6).

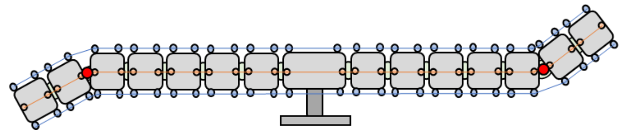

(a) Case of a tipper joint rotated in the vertical plane

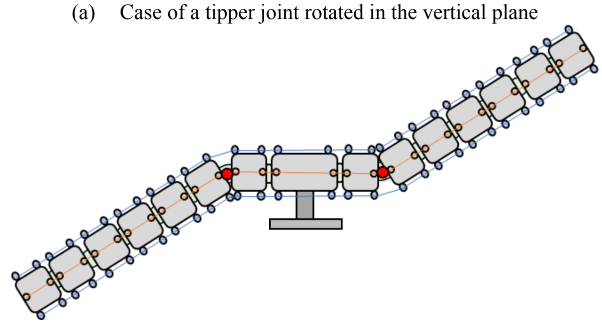

(b) Case of a rooter joint rotated in the vertical plane

Figure 5. Correspondence between active and passive joints

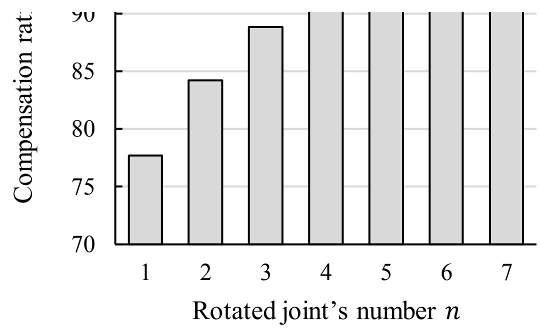

Figure 6. Relationship between the positions of the rotating joint and the gravity compensation ratio

B. Relationship between curvature and gravity compensation ratio

Simulations were employed to estimate the relationship between the bending angles in the proposed mechanism and the gravity compensation ratio ε. Given the large number of degrees of freedom of the proposed mechanism, the sheer number of possible joint angle combinations makes it impractical to investigate all the combinations. Therefore, simulations were conducted under the condition of maintaining a constant curvature for all the joints.

Simulations for the gravity compensation ratio ε were conducted for the proposed mechanism performing constant-curvature flexure in the vertical plane (see Fig. 7). Joint angles θ_n and φ_n were given by

$$\begin{bmatrix} \theta_n \\ \varphi_n \end{bmatrix} = \begin{bmatrix} \Theta \\ 0 \end{bmatrix}. \tag{30}$$

The relationship between the joint angle Θ and the gravity compensation ratio ε under the conditions of equation (30) is investigated (refer to Fig. 8). As a general trend, the gravity compensation ratio ε decreases with an increase in the joint angle Θ. This is likely because the joint-angle errors ($\Delta\theta$) increase with Θ.

The gravity compensation ratio of the proposed mechanism performing constant-curvature bending in three dimensions was calculated (see Fig. 9). Joint angles θ_n and φ_n are given by the following state vector.

$$\boldsymbol{x} = \begin{bmatrix} \theta_n \\ \varphi_n \end{bmatrix} = \begin{bmatrix} \Theta \\ \Phi \end{bmatrix}. \tag{31}$$

The relationship between the state vector $\boldsymbol{x}$ and the gravity compensation ratio ε under the conditions of equation (31) was simulated (Fig. 10). Overall, increasing the joint angle reduced the gravity compensation ratio. This is likely because the joint-angle errors $\Delta\theta$ and $\Delta\varphi$ increased with the joint angle Φ. However, an increase in Φ resulted in an increase in ε in some local regions. From these observations, it is inferred that increasing joint angles Θ and Φ tends to decrease the gravity compensation ratio ε. However, it is presumed that with an appropriate relationship between joint angles Θ and Φ, the decrease in ε can be mitigated even when Θ and Φ are large.

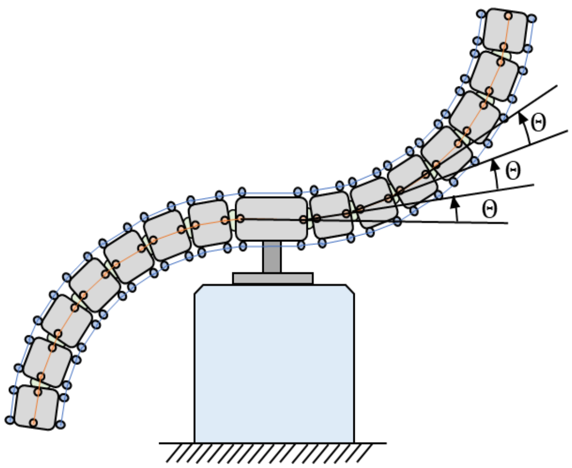

Figure 7. Proposed mechanism performing constant-curvature flexure in the vertical plane

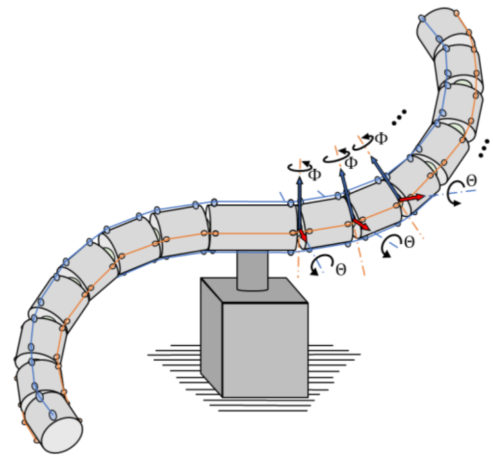

Figure 9. Proposed mechanism performing constant-curvature bending in three-dimensional directions

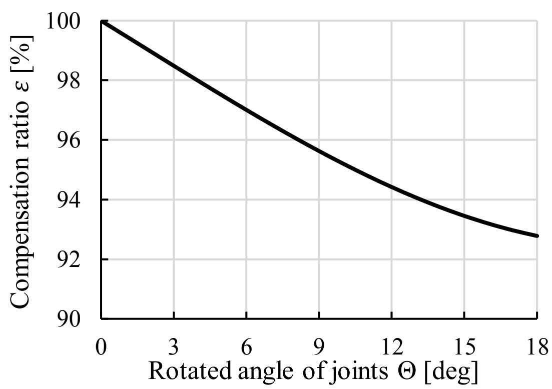

Figure 8. Relationship between the joint angle Θ and the gravity compensation ratio under the conditions of equation (30)

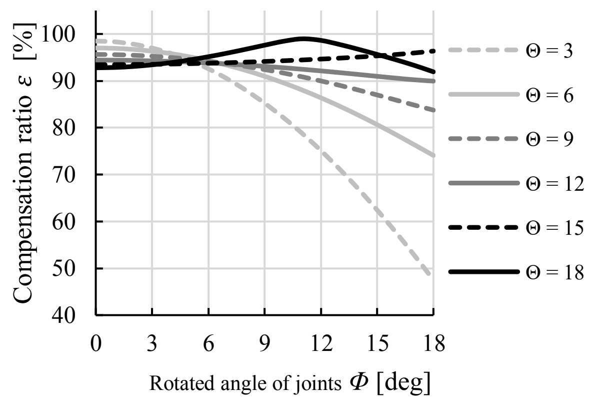

Figure 10. Relationship between the state vector x and the gravity compensation ratio ε under the conditions of equation (31)

IV. Validation Using Prototype

A. Fabrication method for prototype

An actual prototype model was implemented to validate the gravity compensation functionality of the proposed mechanism (Fig. 11). The parameters of the implemented device are as follows.

・Link mass m: 15.2 g

・Link length l: 40 mm

・Wire attachment angle ψ: 10°

・Vertical range of joint: $-18^\circ < \theta_i < 18^\circ$ ($i = 1, \ldots, 7$)

・Horizontal range of joint: $-18^\circ < \theta_i < 18^\circ$ ($i = 1, \ldots, 7$) ・Link material: Acrylic resin

The implemented device featured a hollow structure in each link and joint, allowing the placement of elongated items such as cameras and internal wiring.

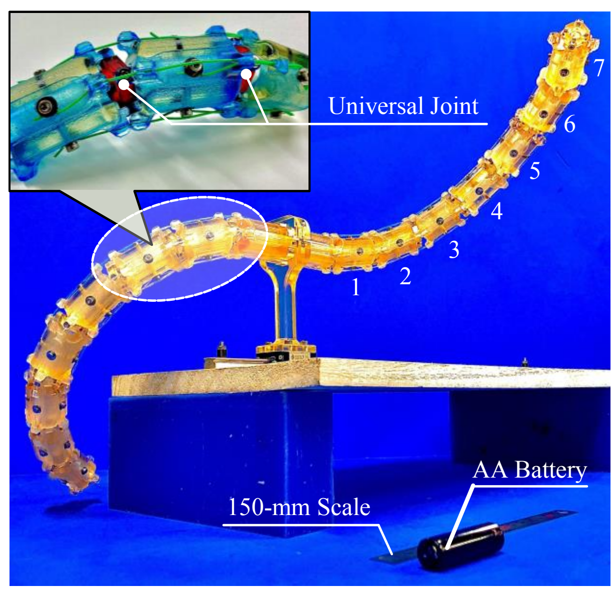

Figure 11. Prototype made of acrylic resin

B. Verification experiment

A simple experiment was conducted to verify the effectiveness of the gravity compensation functionality. In this experiment, each joint of the prototype was manually bent and released to determine whether its posture could be maintained without external support. Additionally, the 0th link was fixed during experiment. The results confirmed that postures with complex curvatures in three-dimensional directions could be sustained even without assistance and it is showed that the proposed mechanism combines practical gravity compensation functionality (see Fig. 11). However, the calculations indicate that this outcome is unrealistic (see Chapter 2). Therefore, it is inferred that in addition to the gravity compensation functionality of the proposed mechanism, other factors such as friction in the joints and wires contribute to posture maintenance.

V. Conclusion

This study introduced the fundamental principles of a multi-joint arm mechanism with gravity compensation inspired by the skeletons of sauropods. Simulations were performed to determine the gravity compensation ratio of the proposed mechanism. Additionally, the effectiveness of the gravity compensation feature was confirmed according to the stability of a prototype.

In future research, we plan to optimize the design parameters and explore configurations for joint angles to increase the energy efficiency. In addition, we aim to apply this mechanism to rescue devices capable of exploring extreme environments and confined spaces (Fig. 12). The theories presented in this paper are applicable irrespective of the size of the mechanism and can be used to achieve versatility in various environments via upscaling or downscaling.

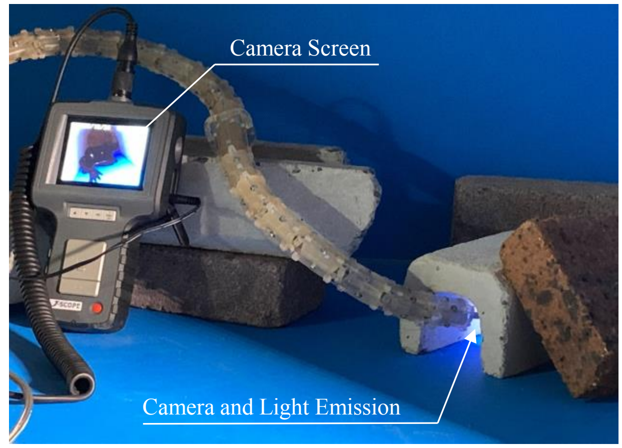

Figure 12. Application of the mechanism to rescue devices capable of exploring extreme environments and confined spaces

References

[1] Y. Tojo, P. Debenest, E. F. Fukushima and S. Hirose: "Robotic system for humanitarian demining–development of weight-compensated partograph manipulator", in Proc. IEEE Int. Conf. on Robotics and Automation, Singapore, 2004, pp.2025–2030.

[2] S. Hirose, T. Ishii and A. Haishi: "Float arm V: hyper-redundant manipulator with wire-driven weight-compensation mechanism", in Proc. IEEE Int. Conf. on Robotics and Automation, pp.368–373, 2003.

[3] M. French and B. Widden: "The spring-and-lever balancing mechanism, George Carwardine and the Anglepoise lamp", in Proc. IMechE Part C: J. Mech. Eng. Sci., 214(3), pp.501–508, 2000.

[4] B. Rogier, S. Mark, D. Wouter and M. W. Boudewijin: "Spring-to-spring balancing as energy-free adjustment method in gravity equilibrators", Journal of Mechanical Design, Vol. 133, Issue 6, 2011.

[5] M. Takeichi, K. Suzumori, G. Endo and H. Nabae: "Development of a 20-m-long giacometti arm with balloon body based on kinematic model with air resistance", Proc. IEEE Int. Conf. on Intelligent Robots and Systems, pp.2710–2716, 2017.

[6] T. Morita, E.F. Kuribara, Y. Shinozawa, S. Sugano: "A novel mechanism design for gravity compensation in three dimensional space", Proc. IEEE Int. Conf. on Advanced Intelligent Mechanics, pp.163–168, 2003.

[7] T. Shen and K. Yano: "An innovative spiral pulley that optimizes cable tension variation for superior balancing performance", Journal of Robotics and Mechatronics, Vol. 34, No. 3, 2022.

[8] K. Koser: "A cam mechanism for gravity-balancing", Mechanics Research Communications, Vol. 36, pp.523–530, 2009.

[9] K. Kaneda and T. Morita: "Realization of mechanical gravity canceller equipped with passive adjustment mechanism for arbitrary load", Transactions of the JSME (in Japanese), Vol. 83, No. 856, pp.1–14, 2017.

[10] R. Sugito and T. Morita: "Self-tuning load compensation mechanism for heavy weight transportation", Proc. JSME Conf. on Robotics and Mechatronics (in Japanese), 2015.

[11] D. Naish and P. Barrett, *Dinosaurs: How They Lived and Evolved*, Washington: Smithsonian Books, 2016.

[12] W. P. Coombs Jr., *Sauropod Habits and Habitats*, Amsterdam: Elsevier Scientific Publishing Company, 1975.

[13] M. P. Taylor and M. J. Wedel, "Why sauropods had long necks; and why giraffes have short necks", *PeerJ*, DOI 10.7717/peerj.36.

[14] R. M. Alexander, *Dynamics of Dinosaurs & Other Extinct Giants*, New York: Columbia University Press, 1989.

[15] A. Horigome, G. Endo and K. Suzumori: "Design of a weight-compensated and coupled tendon-driven articulated long-reach manipulator", Proc. IEEE Int. Symp. on System Integration, pp.598–603, 2016.